Contribution of campaign GNSS toward parsing subsidence rates by time and depth in coastal Bangladesh

Michael Steckler, Md. Hasnat Jaman, Celine Jo Grall, Steven Goodbred, Carol Wilson, Bar Oryan

Contribution of campaign GNSS toward parsing subsidence rates by time and depth in coastal Bangladesh

Michael S. Steckler[1], Md. Hasnat Jaman[2], Céline Jo Grall[1,3], Steven L. Goodbred[4], Carol A. Wilson[5], Bar Oryan[6]

[1] *Lamont-Doherty Earth Observatory of Columbia University, Palisades, NY, USA*
[2] *Department of Geology and Mining, Barisal University, Barisal, Bangladesh and Department of Geoscience, Auburn University, Auburn, AL, USA*
[3] *LIENSs, La Rochelle University, La Rochelle, France*
[4] *Department of Earth and Environmental Sciences, Vanderbilt University, Nashville, TN, USA*
[5] *Department of Geology and Geophysics, Louisiana State University, Baton Rouge, LA, USA*
[6] *Laboratoire de Géologie, Département de Géosciences, École Normale Supérieure, Paris, France.*

Abstract

Coastal regions are vulnerable to rising seas, increasing storm magnitude, and decimation of ecologically fragile areas. Deltas are particularly sensitive to the balance between sea level rise, land subsidence and sedimentation that determine relative elevation. Bangladesh has been highlighted as being at risk from sea level rise, but reliable estimates of land subsidence are limited. Subsidence rates vary spatially, and with depth and time. However, integrating measurements from different methods can approach a more complete understanding of factors controlling spatially and temporally varying rates. To augment our compilation of rates from stratigraphic wells, historic buildings and structures, vertical strainmeters, RSET-MH, and continuous GNSS sites, we resurveyed geodetic monuments in coastal Bangladesh. We resurveyed 48 sites ~18 years after the monuments were installed. Approximately ½ the sites had high rates that we strongly suspected to result from unstable monuments, confirmed by a later resurvey of 4 sites. Remaining sites show subsidence rates of 13-15mm/y, tapering to 0-2mm/y in the northwestern part of the study area. Sites with rates <2 mm/y overlie thin (≤35m), sandy Holocene deposits. Remaining sites overlie thick (70 to >90m) muddy deposits within the incised valleys of the Ganges, Brahmaputra and Meghna Rivers. Together with earlier measurements, we parse the different rates and mechanisms of subsidence. We estimate 2-3mm/y correspond to deep processes, such as isostasy. 1-5mm/y is estimated to result from compaction of Holocene strata, with thicker and muddier strata undergoing greater compaction. Finally, 5-7 mm/y result from shallow, edaphic effects such as tree roots, burrows, organic matter decomposition, and shallow (≤10m) sediment consolidation on short timescales (10^0-10^2y) in the upper few meters. Subsidence rates in areas of active sedimentation, such as rice fields and mangrove forests, are greater than at buildings and structures without active sedimentation. Subsidence on timescales >300y, which does not include edaphic effects, are up to ~5mm/y. We note shallow subsidence can be offset by active deltaic sedimentation, and do not necessarily indicate elevation loss. Collectively, the integration of these approaches allows us to better quantify the varied contributions to land subsidence from edaphic effects, Holocene sediment compaction, lithology, and time.

Keywords: Subsidence, Bangladesh, Ganges-Brahmaputra Delta, GNSS, Holocene

Submitted to Frontiers of Earth Sciences special issue "How does the architecture of Holocene deposits affect land subsidence and saltwater intrusion in coastal areas?", eds. D. Ruberti, P. Minderhoud, L. Tosi, P. Teatini,

1. Introduction

Coastal regions worldwide face an ever-increasing sustainability issue as millions continue to migrate or retreat to these vulnerable regions susceptible to rising seas, storm impacts, and decimation of ecologically fragile areas. Deltas, the low-lying land at river mouths, are particularly sensitive to the dynamic physical forcings, such as the delicate balance between sea-level rise, land subsidence and sedimentation – these are the major parameters governing delta fate and maintaining relative land-surface elevation at the coast (Milliman et al., 1989; Syvitski et al, 2005; Blum and Roberts, 2009; Giosan et al., 2014). However, each of these factors represents an aggregate of multiple, spatiotemporally variable processes that are not often disaggregated into their relevant components – rather, values for sea-level change, subsidence, and sedimentation are typically taken as mean rates of vertical change (units of mm/yr) and applied across entire delta systems, even where significant variations are well recognized (Passalacqua et al., 2021).

Despite their importance in understanding deltaic and coastal system dynamics, mean subsidence rates are most often used, or even maximum rates sometimes (e.g., Ericson et al., 2006; Syvitski et al., 2009; Ostanciaux et al., 2012; Tessler et al., 2015, 2018). This is because the field observations needed to differentiate spatial variations or to disaggregate individual components are difficult to make and have rarely been collected. This data gap represents a major problem for coastal risk assessment, because synoptic to decadal-scale observations for all three of these factors often yield rates that are 2-10x higher than the century to millennial-scale averages most commonly used to predict delta sustainability in the long term (Shirzaei et al., 2021). Furthermore, there is a complex feedback whereby the sedimentation needed to offset elevation loss from subsidence also induces higher subsidence rates from compaction and isostatic loading. Thus subsidence rates are often highest where deltas are receiving the sediments needed to counter it. Given the spatial variability of sediment deposition along deltaic channel networks (e.g., Passalacqua et al., 2013), this means the most rapid and spatially variable factors controlling land elevation are not typically considered in delta morphodynamics and risk assessment models.

In addition, the processes that contribute to subsidence act over different depth ranges. While glacial isostatic adjustment to water and sediment loading impact the entire sediment column, compaction is greatest near the surface and decreases with depth (e.g., Athy, 1930; Terzaghi and Peck, 1967; Sclater and Christie, 1980; Gluyas and Cade, 1997; Kooi and DeVries, 1998; Bahr et al., 2001; Sheldon and Retallack, 2001; Kominz et al., 2011). A substantial portion of high subsidence rates is often due to very shallow sediment compaction and edaphic/ecological factors. For example, Cahoon et al. (1995) examined four sites in the U.S. and found that shallow subsidence in the upper 3-5 m varied from 2 to 25 mm/y with the highest rates in the Mississippi Delta. Their observed subsidence rates correlated closely with the sedimentation rates suggesting that sedimentation was driving shallow compaction. Jankowski et al. (2017) examined 274 sites in the Mississippi Delta and concluded that at least 60% of the total subsidence occurred in the upper 5-10 m, although there was only a weak correlation between the sedimentation and shallow subsidence rates, with considerable scatter. There is also the well-known Sadler effect

(Sadler, 1981) in which sedimentation rates decrease with increasing timescale, as can be seen in subsidence rates measured in the Ganges-Brahmaputra Delta (Brown and Nicholls, 2015).

The variance of subsidence rates and their components occurs in four dimensions across spatial, depth, and temporal scales, and each type of measurement provides an estimate relative to a different datum (Steckler et al., 2022). Thus, measurements of land subsidence are like the fable of the blind men examining an elephant, each system measures part of the story. However, by combining multiple measurements, we can approach a more complete understanding of what is happening. Knowing the current balance of sediment deposition, sediment compaction, tectonic land movement, and isostatic loading is critical for understanding elevation and sediment dynamics in deltas around the world. Here, we focus on the Ganges-Brahmaputra Delta (GBD) and the prospect for near-future land loss and salinization in this megadelta that is home to >200 million people. In this study, we add to a previous synthesis of subsidence measurement in the GBD by Steckler et al. (2022) by adding new results from a campaign GNSS survey of geodetic monuments in coastal Bangladesh. Integrating measurements from different methods (e.g., stratigraphic wells, historic sites, vertical strain meters, RSET-MH [Rod Surface Elevation Tables and Marker Horizons], continuous GNSS and campaign GNSS) allows us to approach a more complete understanding of the factors controlling the spatially and temporally varying rates of subsidence in this delta.

2. Ganges-Brahmaputra Delta

3. Previous Measurements

In general, it is recognized that thick sedimentary deposits loading the lithospheric plate and compacting underlying deposits enhance the subsidence rate, and these rates are inversely time-dependent, with younger deposits consolidating at greater rates commensurate with their age (e.g., Meckel et al., 2007; Tornqvist et al., 2008; Yuill et al., 2009). Previous work studying subsidence in the GBD found this fundamental temporal control also holds true in the GBD (Brown and Nicholls, 2015; Steckler et al., 2022). The Holocene averaged subsidence rates increase from the Hinge Zone of the early Cretaceous passive margin seaward from 0 to 4.5 mm/yr (Grall et al., 2018). The rates derived from 300-600 year old archeological sites are similar to the estimated Holocene rates of 2 to 4 mm/yr (Fig. 1; Sarker et al., 2012; Hanebuth et al., 2013, 2021; Chamberlain et al., 2020b; Steckler et al., 2022). In comparison, Global Navigation Satellite System (GNSS) and tide gauge subsidence rates from the past two decades generally show slightly higher rates than the Holocene averages (4 – 8 mm/y; Figs. 1). Even more recent Rod Surface Elevation Tables coupled with Marker Horizons (RSET-MH) and vertical strainmeters show much higher rates of 9-10 mm/yr (Fig. 1). These instruments, in sites of active sedimentation, include a new spatial component: shallow subsidence that is not recorded by river gauges and GNSS. However, it should be noted that GNSS records deep subsidence, which is not measured by RSETs or strainmeters. Regardless, results collected to present indicate that the amount of ongoing shallow sediment compaction in the GBD is considerable.

Recent InSAR analyses (Higgins et al. 2014; Woods et al., in prep.) suggest that average rates of surface subsidence range from 5 to 10 mm/yr over large areas of the GBD and reach 18 mm/yr in areas of recent channel infilling.

While subsidence rates appear to be driving the rates of Relative Sea Level Rise (RSLR = eustatic SLR + subsidence) in this delta (Steckler et al., 2022), water level fluctuations that drive land surface elevation are also compounded by tidal amplification. A recent study showed that mean high water levels in southwest Bangladesh are rising at rates between 10-20 mm/yr, primarily from poldering and the redistribution of tidal waters (Pethick and Orford, 2013; Bain et al., 2019). While areas still connected to the tides and the supply of sediment appear to be keeping pace with this Effective Sea Level Rise (ESLR= RSLR + tidal amplification; Bomer et al., 2020; Valentine et al., 2021), the impacts delta-wide are poorly resolved. Further, as poldered landscapes appear to be compacting at seasonally high rates due to agricultural land-use changes, flood risk will only increase in these areas over time with ESLR (>60% according to Valentine et al., 2021). We require a better understanding of the elevation and water surface dynamics that are driving delta development, particularly in recent decades with human modification and land-use change.

4. Methods

3.1 Campaign GNSS

Currently there are 38 sites where continuous GNSS measurements have been made in Bangladesh, but only 11 of them are in the coastal zone and not subject to vertical displacement imparted by interseismic motion of the Indo-Burma subduction zone (e.g., Steckler et al., 2016; Mallick et al., 2019; Oryan et al., 2023). While a few sites were established in 2003 and can provide accurate subsidence rates, some sites were only installed in 2019 and the resulting time series is too short to yield accurate rates. The coastal zone GNSS sites are also sparsely located (Fig. 1) and do not provide sufficient coverage to map the spatial variability of the surface vertical motion. However, data from the continuous GNSS sites are supplemented here by new results campaign measurements of some of the 278 geodetic monuments installed throughout Bangladesh by the Survey of Bangladesh (SoB) and the Japan International Cooperation Agency (JICA).). The sites in southern Bangladesh, where subsidence is of greatest concern, were primarily installed in 2001-2002 and can provide a multi-decadal measurement of total subsidence. These sites are relatively densely located at approximately 15-30 km intervals, with a total of 55 sites in southwestern Bangladesh, providing excellent coverage of the region for densifying the subsidence map. The sites were first surveyed by campaign GNSS using a Leica SR9500s with Leiat302-GPs for a duration of 4 hours in 2002. For sites having heavy tree cover or obstructions, a long pole (6.9-9.5 m) stabilized with guy wires was used for the antenna. Most sites were surveyed from January-March, with the remaining sites surveyed the following November-December after the monsoon (Fig. S2).

We resurveyed these sites in January-March 2020 and computed subsidence rates relying on the original survey. Despite the measurements were only conducted twice, in 2002 and 2020, the lengthy span of approximately 18 years between these two observations ensures the accuracy of the resulting subsidence rates is not compromised, assuming linear subsidence over that time span. Additionally, the high number of observation sites enhances the ability to discern patterns in subsidence more clearly.

The field survey took place in several stages as part of the “Long Term Monitoring, Research and Analysis of Bangladesh Coastal Zone (Sustainable Polders Adapted to Coastal Dynamics)” project of the Coastal Embankment Improvement Project (CEIP-1). Our team consisted of personnel from Columbia University, the Institute of Water Modeling, the Survey of Bangladesh,

Dhaka University, the University of Barisal and the French National Research Center (CNRS). One to two survey teams located sites and set up tripods with tribrachs, optical plummets and Trimble NetR9s with Zephyr Geodetic II antennas (Fig. S1). and occupied sites for ~24 hrs, although some were occupied for as long as 3-6 days. For sites where the sky view of the monument was poor due to buildings or trees, we established a nearby GNSS site in an open field and used optical levelling to determine the elevation difference between the monument and the temporary GNSS marker. We were unable to obtain precise measurements because of tree cover at only one site. In some sites a tall monument incompatible with our tripods also required levelling, which generally added an uncertainty of 1 mm to the data. In the Sundarban Mangrove Forest and nearby sites without road access, the survey was conducted during a 10-day boat trip. The slower travel by boat led to the longest observation times. In all, 48 sites were reoccupied while 7 sites had eroded, disturbed, or were otherwise unusable.

We processed the campaign data using GAMIT (Herring et al., 2018), the same software as used for the continuous GNSS sites. We used 16 global reference sites for stabilization, and, for 2020, we also used 2 of our continuous GNSS and a temporary reference site at Barisal University (see Supplement for details). For seasonal vertical motions, we corrected the rates using the seasonal motion at HRNP as a reference (Fig. S2). The results yielded a mixture of rates from very low to quite high. Because measurements only included 1 day in 2002 and usually 2-3 days (range 1-5) in 2020, linearity of the subsidence over that time span is necessarily assumed. The mean difference between the highest and lowest elevations for multiple day observations was 15 mm. The reoccupied sites had a modest median uncertainty of 0.94 mm/y in the vertical, including uncertainties in the equipment setups, predominantly due to the large ~18 y time gap between the occupations. About ½ the sites had rate >20 mm/y or 360 mm over 18 years (Fig. 3). We strongly suspected that the monuments at these sites are unstable and record subsidence or disturbance that is local to the site. Three sites yielded slight uplift, but only at a single site (GPS 2876) is the value beyond the 2σ uncertainty.

To examine whether recorded the highest rates of subsidence recorded are due to monument instability, a team from Barisal University reoccupied four sites near Barisal in October 2020, with two showing moderate rates (13-14 mm/yr) and two showing anomalously high rates (20-28 mm/yr). Both sites exhibiting the moderate rates yielded a colinear trend for the three measurements (Fig. 4 top), suggesting that the recorded rates reflect an accurate long-term stable subsidence of the ground surface. In contrast, both sites with the anomalously higher subsidence rates yielded non-linear subsidence with the October 2020 measurement showing either no subsidence or uplift relative to the previous reoccupation of the site in January 2020 (Fig. 4 bottom). For site GPS 192, we suspect that the monument was initially installed at road level, but subsequently slumped to the adjacent field level, producing additional subsidence, and is currently shifting vertically with the seasonal movements of the rice field. We suggest that other sites exhibiting such high subsidence rates are subject to similar surface instability and are therefore excluded from our analysis.

5. Results

Following the removal of the unstable monument sites from the analysis, the remaining sites show a systematic increase in subsidence from near zero in the NW to ~14-15 mm/y in the southeast (thick gray line in Figure 5). The sites in the northwest that show little to no

subsidence are near Tube Well Transect G where the Holocene sediments are predominantly sandy (average mud content 21 ± 19%), while the remaining sites with higher subsidence rates correspond to the muddier Holocene stratigraphy of Transects H and J/K (average mud content 50± 19% and 55± 15%, respectively; Fig. 6). The muddier stratigraphy of the lower fluvio-tidal deltaplain is therefore likely to be contributing to higher subsidence rates through greater sediment compaction. However, these rates from the campaign monument surveys are considerably higher than those from the continuous GNSS obsservations (yellow box in Figure 4). Since all of the continuous GNSS are installed on reinforced concrete buildings, we interpret that the SoB monuments measured by campaign GNSS are recording shallow subsidence of the sediments that is not observed at the continuous GNSS sites. This interpretation is supported by the subsidence rates at the KHLC compaction meter (Steckler et al., 2022) and at the RSET-MH (Bomer et al., 2020; Akter et al., in review) located in the Sundarbans just south of Polder 32 (pink box in Figure 4). These compaction meter and RSET-MH rates of 9-11 mm/y are slightly less than the campaign GNSS sites reported here, but higher than the continuous GNSS sites reported by Steckler et al. (3-7 mm/yr; 2022). The RSET-MH within Polder 32, where sedimentation rates are low, yields 5 mm/y of shallow subsidence (Akter et al., in review), suggesting that a significant part of the shallow subsidence is due to compaction. The compaction vs. depth profile at the KHLC site shows that all of the observed compaction is only occurring in the Holocene sediments alone, with no compaction in the Pleistocene strata between 100 and 300 m depth. We therefore interpret the difference between the KHLC and the RSET-MH sites, and the campaign GNSS measurements to be the deep subsidence recorded by the continuous GNSS, but not other two systems.

To further investigate the influence of compaction, Figure 7 shows the pattern of subsidence from the campaign GNSS compared to the thickness of Holocene sediments mapped by over 500 hand-drilled tube wells (Sincavage, 2017; Sincavage et al., 2017; Grall et al., 2018; Raff et al., 2023). During the Last Glacial Maximum (LGM), the major rivers of the GBD incised significant valleys feeding into the shelf-indenting Swatch of No Ground (SoNG) canyon (Fig. 7, Pickering et al., 2018), where the thickest Holocene sediments are found (Palamenghi, 2011). Exposure and weathering of the interfluves created an oxidized clay paleosol (Umitsu, 1993) that has been mapped by Hoque et al. (2014). The Last Glacial Maximum Paleosol (LGMP) surface has been added in shades of brown in Figure 7, where it is found in outcrop and in the subsurface. The resulting patterns reveal that all of the low subsidence sites (<5 mm/y) are located where relatively thin Holocene sediments (30-40 m) overlie the LGMP, whereas the higher rates are associated with thicker sediments in the paleo valleys (>60 m). Holocene thicknesses at these sites are likely 30-40 m. The two intermediate sites (5-10 mm/y) also overly the mapped paleosol, but where it may be deeper (60-85 m) as they lie near well with the LGMP at that depth and ones where its was too deep to reach. The campaign GNSS sites with the fastest subsidence rates all lie within the individual incised valleys or the broad confluence of the Ganges, Brahmaputra and Meghna paleo valleys.

The relationship between lithology and Holocene sediment thickness further shows correlation with the campaign GNSS subsidence rates (Fig. 8). Where the Holocene sediment thickness is greater than the maximum depth of tube wells, maximum depth to Pleistocene was roughly estimated using the incised valley pathways and the LGM depth of the SoNG canyon (>500 m; Palamenghi, 2011). There is a clear relationship of increasing subsidence with sediment thickness up to ~100 m, although rates at campaign GNSS sites with sediment thickness >100 m do not appear to increase further. The plot symbols are also colored by the fraction of mud

(interpolated) in the Holocene stratigraphy, showing that higher mud fraction also correlates with faster subsidence rates. Since the sandier Holocene sediments that lie upstream are also thinner compared with the thicker and muddier Holocene sediments of the lower delta (Figures 5 and 6), we cannot parse out the relative importance of Holocene mud content versus sediment thickness with the current data.

6. Discussion

Understanding the current balance of regional and deep processes vs. local and shallow processes such as sediment deposition, sediment compaction, tectonic land movement, and isostatic loading is critical for understanding elevation and sediment dynamics in the GBD and the prospect for near-future land loss and salinization (Raff et al., 2023). Previous research on subsidence measurements made using different methodologies in the GBD shows that variations exhibit systematic spatio-temporal patterns (Grall et al., 2018; Steckler et al., 2022). In general, it is recognized that thick sedimentary deposits loading the lithospheric plate and compacting underlying deposits are found to enhance the subsidence rate, and these rates are inversely time-dependent, with younger deposits consolidating at greater rates commensurate with their ages. Steckler et al. (2022) found this fundamental temporal control also holds true in the GBD. The Holocene averaged subsidence rates increase from near zero at the Hinge Zone of the early Cretaceous passive margin (Fig. 1) to the southeast toward the sea (4.5 mm/yr; Grall et al., 2018). The rates at 300-600 year old archeological sites are similar to the estimated Holocene rates (3–4 mm/yr) at those locations (Fig. 1; Sarker et al., 2012; Hanebuth et al., 2013, 2021; Chamberlain et al., 2020b). In comparison, Global Navigation Satellite System (GNSS) and river gauge subsidence rates (Becker et al., 2020) from the past two decades generally show slightly higher rates than the Holocene (4–7 mm/y; Fig. 1), with the highest rates in the muddy Sundarban Mangrove Forest near the coast. Rod Surface Elevation Tables coupled with Marker Horizons (RSET-MH) and vertical strainmeters show much higher rates of 9-11 mm/yr (Bomer et al., 2020; Steckler et al., 2022; Fig. 1). These instruments, in sites of active sedimentation, include a new spatial component: shallow subsidence that is not recorded by river gauges and GNSS. However, it should be noted that GNSS measurements include deep subsidence beneath the monument, which is not captured by the data collected from the RSETs or strainmeters. Regardless, the high rates of the RSET-MH and strainmeter results present indicate that there is a considerable amount of ongoing shallow sediment compaction. Akter et al. (submitted) demonstrates that within an embanked island of coastal Bangladesh where sedimentation is limited, the shallow subsidence is significantly lower than in the adjacent Sundarban Mangrove Forest where sedimentation is rapid (5.0 ± 1.7 versus 8.7 ± 1.2 mm/y, respectively).

Spatially, decadal continuous GNSS subsidence rates are within a millimeter per year of the Holocene rates near the Arial Khan River/Tetulia Channel (Fig. 1), the 17-19th century course of the Ganges River. Prior to the mid 17th century, the Ganges mainstem was along the Hooghly River in West Bengal, India and since the late 19th century it flows down the Lower Meghna River with the Brahmaputra River (Fig. 1; Rennell, 1776; Majumdar, 1942; Eaton, 1993). West of the distributaries branching off the Lower Meghna River, however, continuous GNSS subsidence rates are consistently a few mm/yr greater than the longer-term rates (Fig. 1). Steckler et al. (2022) previously hypothesized that this difference was due to ongoing sediment compaction in the muddier sediment deposited in the interfluves between the mainstem mouths of the Hooghly (Ganges) and Lower Meghna (Ganges and Brahmaputra) Rivers.

Our new data from the campaign GNSS Survey of Bangladesh benchmarks subsidence rates also appear to further support the hypothesis that sediment thickness and lithology are major controlling factors of subsidence rates (Figs. 6-8). Measurements of the subsidence rates from 2002 (date of installation) to 2020 (date of second measurement) revealed very low rates in the NW part of the study area where five sites (Fig. 5, 7; GPS 101, +0.21±1.41; GPS 115, -1.23±1.40; GPS 118, -2.48±1.30; GPS 199, +0.67±2.20; and 2876, +2.93±2.06) show minimal subsidence. Two of these sites show slight uplift, but only the value from site 2876 shows uplift that is greater than the one sigma uncertainty, but it is still less than 2 sigma. These five sites all correspond to areas having thin (~30 m), sandy Holocene stratigraphy with a low mud fraction (8-15 %) of mud lithology (Table S3; Fig. 6-8). Moving seaward, the campaign GNSS sites yield subsidence rates that are much greater (11-15 mm/yr). These highest rates correspond to the coalesced incised valleys where the Holocene sediment thickness filling is over 91 m and is considerably muddier than upstream (51±8% mud content; Fig. 6, 8). These high rates are greater than either the continuous GNSS or RSET/KHLC measurements reported by Steckler et al. (2022; Fig. 5). The campaign GNSS measurements include both shallow and deep compaction/subsidence, while the GNSS contains only the deeper subsidence and the RSETs the only shallow subsidence. We note that most of the sites in the Sundarbans Mangrove Forest yielded high rates (11, 19, 22, 23, 24, 28, 31, 40 mm/y). It is possible that some of these higher rates could be accurate due to the high sedimentation rates of the muddy sediments there (Rogers et al., 2013; Rogers and Overeem, 2017; Bomer et al., 2020a; Akter et al., submitted). This possibility will be examined in future fieldwork and modeling efforts.

Combining these different measurements that sample overlapping combinations of shallow and deep subsidence--and that do or do not include near surface soils--we can begin to differentiate the depth range for the various components of subsidence. Parsing the subsidence rates to get at these discrete contributions, we estimate that the deep subsidence that is generated below the Holocene strata is 2-3 mm/y (Fig. 9). This deep-subsidence component in delta systems is generally recognized as sediment isostasy associated with thick sedimentary deposits (Karpytchev et al. 2018; Krien et al. 2019). Sediment compaction at great depths is expected to be small because Pleistocene sediments beneath the incised river valleys (>100 m; Sincavage et al., 2017; Grall et al., 2018) already experienced prior loading and will not start to compact again until the weight of any new sediment exceeds the previous overburden reached prior to valley incision (Chapman, 1983). As a result, for most of the incised valleys, little to no compaction of the sediment below the lowstand erosion surface Holocene is expected. Exposure and weathering of the lowstand surface that created the LGMP (Umitsu, 1993; Hoque et al., 2014) also likely reduced the sediment porosity and its susceptibility to compaction.

For the shallowest depths (<10-20 m), we estimate the contribution to the subsidence rates to be up to 5-7 mm/yr (Fig. 9). This conclusion is estimated using previously reported and newly updated RSET-MH measurements, the KHLC measurements, and the increased subsidence rate of the campaign GNSS relative to the continuous sites (Fig. 9). While RSET-MH results show similar average shallow subsidence rates as KHLC (Bomer et al., 2020a; Akter et al, in review), we note there is a higher shallow subsidence rate in the mangrove forest (7-11 mm/yr) compared to anthropogenically modified areas (3-7 mm/y; Akter et al., in review). We suggest that, the higher sediment accumulation rate in the Sundarban Mangrove Forest versus poldered areas (25 mm/y vs 11 mm/yr) is driving shallow compaction and is the cause of this difference (Akter et al., submitted).

The RSET rates apply to the depth of the instrumentation, i,e., the upper 24 m. There is additional subsidence deeper in the Holocene below the base of the RSET rod (*sensu* Jankowski et al., 2017). This means that the KHLC subsidence rate of 9 mm/y (Steckler et al., 2022) is greater than the shallow subsidence in the polder (3-7 mm/y Akter et al., in review) because it extends to 100 m, beyond the depth of the RSET rods. Thus, at intermediate depths, perhaps corresponding to the Holocene sediment thickness of up to a few hundred meters (Fig. 9), we estimate 1-4 mm/y.

These values of shallow subsidence are similar to observations at the Mississippi Delta where estimates of 3-6 mm/y were found (Jankowski et al., 2017; Karegar et al., 2020). The high rates of shallow subsidence in the Mississippi delta are likely due to the consolidation of organic-rich and muddy strata in the upper 10 m or less (Jankowski et al., 2017; Keogh et al., 2021). In the GBD with its large tidal range and highly seasonal water stage, most organic matter is consumed or oxidized such that there is little organic matter preservation deeper than ~5 m (Allison et al., 2003; Bomer et al., 2020b; Goodbred et al., 2003). This loss of mass through organic degradation and wood extraction (Auerbach et al., 2015) and the collapse of large void spaces such as faunal burrows may contribute to the sizeable very shallow subsidence (Bomer et al., 2020a; 2020b).

Finally, we note that the high rates of total subsidence obtained by the campaign GNSS measurements (11-15 mm/y) do not necessarily indicate that there is elevation loss in the GBD. The most critical factor for the population is the net change in elevation relative to sea level. The sedimentation rates in active depositional areas of 25 mm/y in the mangroves (Rogers et al., 2013; Rogers and Overeem, 2017; Akter et al., submitted) appear to be sufficient to keep pace with subsidence and sea level rise. However, the rates of sedimentation within the polders, with constrained riverine deposition (11 mm/yr; Akter et al., submitted) indicate that these areas are at risk of elevation loss, as has been previously documented (Auerbach et al., 2015). Better understanding of elevation change and its variation throughout the delta, in addition to our subsidence analysis, is seriously needed.

7. Conclusions

Previous global studies used single values for the subsidence of the GBD (Ericson et al., 2006; Syvitski et al., 2009; Ostanciaux et al., 2012), although compilations (Brown and Nicholls, 2015) show a wide range of apparent subsidence. New data presented here is beginning to refine our understanding of subsidence rates in the GBD by enabling us to parse out contributions from multiple measurement systems operating at different spatial and temporal scales and depth ranges (Fig. 9). GNSS on building measure the total deeper subsidence, but miss shallowest subsidence above the depth of foundation/pilings of the building. The subsidence rates from the continuous GNSS (Fig. 1; 3-7 mm/y) are similar to both the rates estimate for the region by tide gauge analysis (Becker et al., 2020), and average Holocene subsidence (Grall et al., 2018), although the distribution has some differences. However, the continuous GNSS rates are a few millimeters/year higher in the southwest coastal zone due to greater compaction of muddier sediments found there. The similarity of rates for these methods indicates that the anchoring of the tide gauges also excludes the shallowest component of subsidence.

In contrast, methods that include very shallow subsidence, such as the RSET-MH, KHLC compaction meter, and the campaign GNSS survey yield much higher rates (Fig. 1, 3, 5, 7). The RSET-MH measure all of the subsidence above the base of the rods (≤ 24 m). The optical fiber

compaction meter wells each measure to the base of the well revealing compaction within the Holocene, which is 90-100 m thick at the site. The campaign GNSS at Survey of Bangladesh (SoB) monuments measure the total subsidence, but some sites include disturbances that increased the apparent local subsidence of the monuments and were excluded (Fig. 3, 4). Using the combination of these tools, we create a preliminary estimate of subsidence in three depth zones.

For the deepest zone, we estimate 2-3 mm/y of subsidence (Fig. 9). This includes both sediment isostasy and any deeper sediment compaction. In the intermediate zone above the base of the RSETs at ~24 m or Holocene, but below the foundations of the building at a few meters, we find 1-4 mm/y of subsidence. Values of 1 mm/y correspond to regions with a sandier lithology, while compaction for muddier regions is likely 3-4 mm/y. Together, they comprise the Holocene rates of 1-5 mm/y across the region found by Grall et al. (2018) and seen in historic sites (Steckler et al., 2022). The shallowest region of the upper few meters may have subsidence rates as large as 5-7 mm/y corresponding to the dewatering of freshly deposited muds at the surface, collapse of burrows, and decay of organic matter including roots. These estimates are preliminary and subject to change as we obtain additional data from the more recent GNSS and RSET-MH installed in 2019. Additional measurements of lithology and porosity near the RSET and SoB monuments will further help refine estimates of the shallowest subsidence.

The highest rates of total subsidence are 11-15 mm/y, which includes compaction of the shallowest soils. These rates correspond to areas with active sediment deposition, and this sedimentation drives the shallowest compaction. These high rates do not imply elevation loss as sedimentation rates are still higher than subsidence rates (Rogers et al., 2013; Rogers and Overeem, 2017; Akter et al., submitted). However, the interior of polders, where sedimentation is limited have seen significant elevation loss that has resulted in drainage problems (Auerbach et al., 2015; Akter et al., submitted). At the polder embankments, site preparation and lack of sedimentation would eliminate the shallowest subsidence. We therefore expect that polder embankments and buildings should see subsidence rates comparable to the continuous GNSS on buildings (1-7 mm/y). However, this subsidence that is not compensated by sedimentation at the anthropogenically-modified polder sites. Quantified subsidence rates do vary across coastal Bangladesh in somewhat tractable regional patterns (see Fig. 1, 5, 7), but we show they also vary locally depending on the depositional setting and the extent of anthropogenic modification.

8. Acknowledgements

This work was supported by BWDB contract CEIP-1/C3/C4 “Long Term Monitoring, Research and Analysis of Bangladesh Coastal Zone (Sustainable Polders Adapted to Coastal Dynamics)” project of the Coastal Embankment Improvement Project (CEIP-1) contract. We would like to thank the Survey of Bangladesh, particularly Debashish Sarker, for assistance with data access. We also thank all of the participants in the fieldwork, Salam Sikder, Shaikh Nahiduzzaman, and Muktidir Sober of the Institute for Water Modeling; Ershadul Mondal of the Survey of Bangladesh; Nahin Rezwan, Md. Saiful Islam, Md. Yeasin Arafath, Md. Wabidur Rahman, Md. Ashik Afroz, Shahriar Kabir Shoaeb, Md. Rakibul Islam, Md. Galib Muttaki of Barisal University; and Masud Rana, Md. Shahadat Hossain Biplab and Sanju Singha of Dhaka University

9. Conflict of Interest

The authors declare that the research was conducted in the absence of any commercial or financial relationships that could be construed as a potential conflict of interest.

9. Author Contributions

M.S.S. conceptualization, data acquisition and analysis, writing; M.H.J. data acquisition, editing; C.J.G. data acquisition, data analysis, editing; S.L.G. data analysis, writing, editing; C.A.W. data analysis, writing, editing B.O. data processing, editing

10. References

Akter, S., C.A. Wilson, A.H. Bhuiyan, S.H. Akhter, M.S. Steckler, Md.M. Rana (submitted). Comparison of surface elevation change, vertical accretion & shallow subsidence between polders and the natural Sundarbans of the Ganges-Brahmaputra delta plain, Estuaries and Coasts, Special Issue *Current Advances in Coastal Wetland Elevation Dynamics*, D. Cahoon & G. Guntenspergen (eds.).

Allison, M.A., Khan, S.R., Goodbred Jr, S.L. and Kuehl, S.A., 2003. Stratigraphic evolution of the late Holocene Ganges–Brahmaputra lower delta plain. *Sedimentary Geology*, *155*(3-4), pp.317-342.

Athy, L.F., 1930. Density, porosity, and compaction of sedimentary rocks. Bull. Am. Ass. Petrol. Geol., 14: 1-24.

Auerbach, L., Goodbred, S., Mondal, D., Wilson, C., Ahmed, K.R., Roy, K., Steckler, M., Small, C., Gilligan, J., Ackerly, B. (2015). Flood risk of natural and embanked landscapes on the Ganges–Brahmaputra tidal delta plain. Nature Climate Change 5, 153-157, doi: 10.1038/nclimate2472.

Bahr, D.B., Hutton, E.W.H., Syvitski, J.P.M., Pratson, L.F., 2001. Exponential approximations to compacted sediment porosity profiles. Computers & Geosciences 27, 691–700.

Bain, R.L., Hale, R.P., Goodbred, S.L., 2019. Flow Reorganization in an Anthropogenically Modified Tidal Channel Network: An Example From the Southwestern Ganges-Brahmaputra-Meghna Delta. J. Geophys. Res. Earth Surf. 124, 2141–2159. https://doi.org/10.1029/2018JF004996

Becker, M., F. Papa, M. Karpytchev, C. Delebecque, Y. Krien, J.U. Khan, V. Ballu, F. Durand, G. Le Cozannet, A.K.M.S. Islam, S. Calmant, C.K. Shum (2020) Water level changes, subsidence, and sea level rise in the Ganges–Brahmaputra–Meghna delta, Proceedings of the National Academy of Sciences, 117 (4) 1867-1876; doi:10.1073/pnas.1912921117.

Blum M.D., Roberts, H.H. (2009) Drowning of the Mississippi Delta due to insufficient sediment supply and global sea-level rise. Nat. Geosci. 2: 488–491. doi:10.1038/NGEO553

Bomer, E.J., Wilson, C.A., Hale, R.P., Hossain, A.N.M., and Rahman, F.M.A. (2020a). Surface elevation and sedimentation dynamics in the Ganges-Brahmaputra tidal delta plain, Bangladesh: implications for the sustainability of natural and human-impacted coastal systems. *Catena.*187:104312.

Bomer, E.J., Wilson, C.A. and Elsey-Quirk, T., 2020b. Process controls of the live root zone and carbon sequestration capacity of the Sundarbans Mangrove Forest, Bangladesh. *Sci*, *2*(3), p.54.

Brown, S., R. J. Nicholls, Subsidence and human influences in mega deltas: The case of the Ganges-Brahmaputra-Meghna. Sci. Total Environ. 527–528, 362–374 (2015).

Cahoon, D.R., D.J. Reed, and J.W. Day. 1995. Estimating shallow subsidence in microtidal salt marshes of the southeastern United States: Kaye and Barghoorn revisited. Mar. Geol. 128:1–9. doi:10.1016/0025-3227(95)00087-F

Chamberlain, E.L., S.L. Goodbred, R. Hale, M.S. Steckler, J. Wallinga, C. Wilson (2020). Integrating geochronologic and instrumental approaches across the Bengal Basin, Earth Surface Processes and Landforms, 45, 56-74., https://doi.org/10.1002/esp.4687.

Eaton, Richard M. The Rise of Islam and the Bengal Frontier, 1204-1760. Berkeley: University of California Press, 192pp.

Ericson, J.P., Vörösmarty, C.J., Dingman, S.L., Ward, L.G., Meybeck, M., 2006. Effective sealevel rise and deltas: causes of change and human dimension implications. Glob. Planet. Chang. 50, 63–82. http://dx.doi.org/10.1016/j.gloplacha.2005.07.004.

Giosan, L, J. Syvitski, S. Constantinescu and J. Day (2014). Protect the world's deltas. Nature 516, 31–33.

Gluyas, J. and C.A. Cade, (1997). Prediction of porosity in compacted sands, AAPG Memoir 69: Reservoir Quality Prediction in Sandstones and Carbonates, Edited by J.A. Kupecz, J. Gluyas, and S. Bloch, 19-27.

Goodbred, Jr., S.L., Kuehl, S.A., Steckler, M., and Sarker, M.H., 2003. Controls on facies distribution and stratigraphic preservation in the Ganges-Brahmaputra delta sequence. Sedimentary Geology, 155:301-316. https://doi.org/10.1016/S0037-0738(02)00184-7

Grall, C., M.S. Steckler, J.L. Pickering, S. Goodbred, R. Sincavage, C. Paola, S.H Akhter, V. Spiess (2018) A base-level stratigraphic approach to determining Holocene subsidence of the Ganges–Meghna–Brahmaputra Delta plain. Earth and Planetary Science Letters, Earth and Planetary Science Letters 499, 23–36, 10.1016/j.epsl.2018.07.008.

Hanebuth, T.J.J., Kudrass, H.R., Linstaedter, J., Islam, B., Zander, A.M., 2013. Rapid coastal subsidence in the central Ganges–Brahmaputra Delta (Bangladesh) since the 17th century deduced from submerged salt-producing kilns. Geology 41 (9), 987–990. http://dx.doi.org/10.1130/G34646.1.

Hanebuth, T.J.J., Kudrass, H.R., Zander, A.M., Akhter, H.S., Neumann-Denzau, G., Zahid, A., 2021. Stepwise, earthquake-driven coastal subsidence in the Ganges–Brahmaputra Delta (Sundarbans) since the eighth century deduced from submerged in situ kiln and mangrove remnants. Nat. Hazards. https://doi.org/10.1007/s11069-021-05048-2

Herring, T.A., R.W. King, M.A. Floyd, S.C. McClusky, 2018. Introduction to GAMIT/GLOBK Release 10.7, 54p.

Higgins, S.A., Overeem, I., Steckler, M.S., Syvitski, J.P.M., Seeber, L., Akhter, S.H., 2014. InSAR measurements of compaction and subsidence in the Ganges–Brahmaputra Delta, Bangladesh. J. Geophys. Res. Earth Surf. 119 (8). http://dx.doi.org/10.1002/ 2014JF003117 (2014JF003117).

Hoque, M.A., McArthur, J.M. & Sikdar, P.K. Sources of low-arsenic groundwater in the Bengal Basin: investigating the influence of the last glacial maximum palaeosol using a 115-km traverse across Bangladesh. *Hydrogeol J* **22**, 1535–1547 (2014). https://doi.org/10.1007/s10040-014-1139-8

Jankowski, K.L., Törnqvist, T.E., Fernandes, A.M., 2017. Vulnerability of Louisiana's coastal wetlands to present-day rates of relative sea-level rise. Nat. Commun. 8, 14792. https://doi.org/10.1038/ncomms14792.

Karegar, M. A., Larson, K. M., Kusche, J., & Dixon, T. H. (2020). Novel quantification of shallow sediment compaction by GPS interferometric reflectometry and implications for flood susceptibility. Geophysical Research Letters, 47, e2020GL087807. https://doi.org/10.1029/2020GL087807

Karpytchev, M., Ballu, V., Krien, Y.,Becker, M., Goodbred, S., Spada, G., Calmant, S., Shum, C., and Z. Khan (2018). Contributions of a strengthened early Holocene monsoon and sediment loading to present-day subsidence of the Ganges-Brahmaputra Delta. Geophysical Research Letters,45,1433–1442. doi.: 10.1002/2017GL076388.

Keogh, M.E., Törnqvist, T.E., Kolker, A.S., Erkens, G. and Bridgeman, J.G., 2021. Organic matter accretion, shallow subsidence, and river delta sustainability. *Journal of Geophysical Research: Earth Surface*, *126*(12), p.e2021JF006231.

Kominz M.A., K. Patterson, and D. Odette (2011). Lithology dependence of porosity in slope and deep marine sediments, Journal of Sedimentary Research, 2011, 81, 730–742, doi: 10.2110/jsr.2011.60.

Kooi, H., DeVries, J.J., 1998. Land subsidence and hydrodynamic compaction of sedimentary basins. Hydrology and Earth System Sciences 2, 159–171.

Krien, Y., M. Karpytchev, V. Ballu, M. Becker, C. Grall, S. Goodbred, S. Calmant, C.K. Shum, and Z. Khan (2019) Present-day subsidence in the Ganges-Brahmaputra-Meghna delta: Eastern amplification of the Holocene sediment loading contribution. Geophys. Res. Lett. 49, 10764–10772.

Mallick, R., Lindsey, E. O., Feng, L., Hubbard, J., Banerjee, P., & Hill, E. M., (2019), Active convergence of the India‐Burma‐Sunda plates revealed by a new continuous GPS network, *Journal of Geophysical Research: Solid Earth*,124, 3155–317, doi: 10.1029/2018JB016480.

Majumdar, S.C. (1942). Rivers of the Bengal Delta, Calcutta University Press, Calcutta, 128pp.

Milliman J.D., J.M. Broadus and F. Gable, (1989). Environmental and Economic Implications of Rising Sea Level and Subsiding Deltas: The Nile and Bengal Examples. Ambio, 18, 340-345.

Ostanciaux, É., Husson, L., Choblet, G., Robin, C., Pedoja, K., 2012. Present-day trends of vertical ground motions along the coast lines. Earth Sci. Rev. 110, 74–92. doi.org/10.1016/j.earscirev.2011.10.004.

Passalacqua, P., S. Lanzoni, C. Paola, and A. Rinaldo (2013), Geomorphic signatures of deltaic processes and vegetation: The Ganges-Brahmaputra-Jamuna case study, Journal of Geophysical Research: Earth Surface, 118(3), 1838–1849, doi:10.1002/jgrf.20128.

Passalacqua, P., Goodbred, S., Giosan, L., Overeem, I., 2021. Stable ≠ Sustainable: Delta dynamics versus the human need for stability, Earth's Future. 10.1029/2021EF002121

Pethick, J. and Orford, J.D. (2013). Rapid rise in effective sea-level in southwest Bangladesh: Its causes and contemporary rates. Global Planetary Change 111: 237–245. doi: 10.1016/j.gloplacha.2013.09.019

Raff, J. L., S.L. Goodbred Jr, J.L. Pickering, R.S. Sincavage, J.C. Ayers, M.S. Hossain, C.A. Wilson, C. Paola, M.S. Steckler, D.R. Mondal, J.-L. Grimaud, C.J. Grall, K.G. Rogers, K.M. Ahmed, S.H. Akhter, B.N. Carlson, E.L. Chamberlain, M. Dejter, J.M. Gilligan, R.P. Hale, M.R. Khan, Md.G. Muktadir, Md.M. Rahman and L.A. Williams (2023). Sediment delivery to sustain the Ganges-Brahmaputra delta under climate change and anthropogenic impacts. Nature Communications, 14(1), 2429, https://doi.org/10.1038/s41467-023-38057-9.

Rennell, R. (1776). An actual survey of the provinces of Bengal, Bahar &c., printed by Andrew Drury, 1 sheet.

Rogers, K.G., S.L. Goodbred, D.R. Mondal, 2013. Monsoon sedimentation on the 'abandoned' tide-influenced Ganges-Brahmaputra delta plain, Estuarine, Coastal and Shelf Science 131, 297-309, http://dx.doi.org/10.1016/j.ecss.2013.07.014

Rogers, K., & Overeem, I. (2017). Doomed to drown? Sediment dynamics in the human-controlled floodplains of the active Bengal Delta. Elementa Science of the Anthropocene, 5, 66. Doi: 10.1525/elementa.250

Sadler, P.M., 1981. Sediment accumulation rates and the completeness of stratigraphic sections. J. Geol. 89, 569–584.

Sarker, M.H., Choudhury, G.A., Akter, J., Hore, S.K., 2012. Bengal Delta Not Sinking at a Very High Rate. Daily Star (23rd December 2012).

Sclater, J. G., and Christie, P. A. (1980), Continental stretching; An explanation of the post Mid-Cretaceous subsidence of the central North Sea basin: Journal of Geophysical Research, 85, 3711-3739.

Sheldon, N.D. and G.J. Retallack (2001). Equation for compaction of paleosols due to burial. Geology, 29, 247–250.

Shirzaei, M., J. Freymueller, T.E. Törnqvist, D.L. Galloway, T. Dura and P.S.J. Minderhoud (2021) Measuring, modelling and projecting coastal land subsidence, Nature Reviews Earth & Environment, 2, 40-58, https://doi.org/10.1038/s43017-020-00115- x

Sincavage, R. (2017). The Holocene sedimentary archive of Sylhet basin, Bangladesh: Linking surface processes to the stratigraphic record within a mass balance framework. PhD dissertation, Vanderbilt University.

Sincavage R., Goodbred, S., and Pickering, J., (2017) Holocene Brahmaputra River path selection and variable sediment bypass as indicators of fluctuating hydrologic and climate conditions in Sylhet Basin, Bangladesh: Basin Research, 30, 302–320, doi:10.1111/bre.12254. 2017

Steckler, M.S., B. Oryan, C.A. Wilsan, C. Grall, S.L. Nooner, D.R. Mondal, S.H. Akhter, S. DeWolf, S.L. Goodbred, Synthesis of the Distribution of Subsidence of the Lower Ganges-Brahmaputra Delta, Bangladesh, Earth-Science Reviews, 224, 103887, doi:10.1016/j.earscirev.2021.103887.

Syvitski, J.P.M., Kettner, A.J., Overeem, I., Hutton, E.W.H., Hannon, M.T., Brakenridge, R.G., Day, J., V r smarty, C., Saito, Y., Giosam, L., Nicholls, R.J., 2009. Sinking deltas due to human activities. Nat. Geosci. 2 (10), 681–686. http://dx.doi.org/10.1038/ngeo629.

Syvitski J.P.M., Vörösmarty, C.J., Kettner, A.J., Green, P. (2005) Impact of humans on the flux of terrestrial sediment to the global coastal ocean. Science 308:376–380. doi:10.1126/science.1109454

Terzaghi, K., Peck, R.B. (1967). Soil Mechanics in Engineering Practice, 2nd ed. Wiley, New York, 729pp.

Tessler, Z., C. J. Vörösmarty, M. Grossberg, I. Gladkova, H. Aizenman, J.P.M. Syvitski, E. Foufoula-Georgiou (2015). Profiling risk and sustainability in coastal deltas of the world. Science, 349 (6248), 638-643.

Tessler, Z. D., C. J. Vörösmarty, I. Overeem and J. P. Syvitski (2018) A model of water and sediment balance as determinants of relative sea level rise in contemporary and future deltas. Geomorphology.

Umitsu, M., 1993. Late Quaternary sedimentary environment and landforms in the Ganges delta. Sedimentary Geology 83, 177–186.

Valentine, L., C.A. Wilson, M. Rahman (2021). Flood Risk of Embanked Areas and Potential Use of Dredge Spoils as Mitigation Measures in the Southwest Region of the Ganges-Brahmaputra-Meghna Delta, Bangladesh, Earth Surface Processes and Landforms, https://doi.org/10.1002/esp.5303

Van Maren, D.S., Beemster, J.G.W., Wang, Z.B., Khan, Z.H., Schrijvershof, R.A. and Hoitink, A.J.F., 2023. Tidal amplification and river capture in response to land reclamation in the Ganges-Brahmaputra delta. *Catena*, *220*, p.106651.

Figures

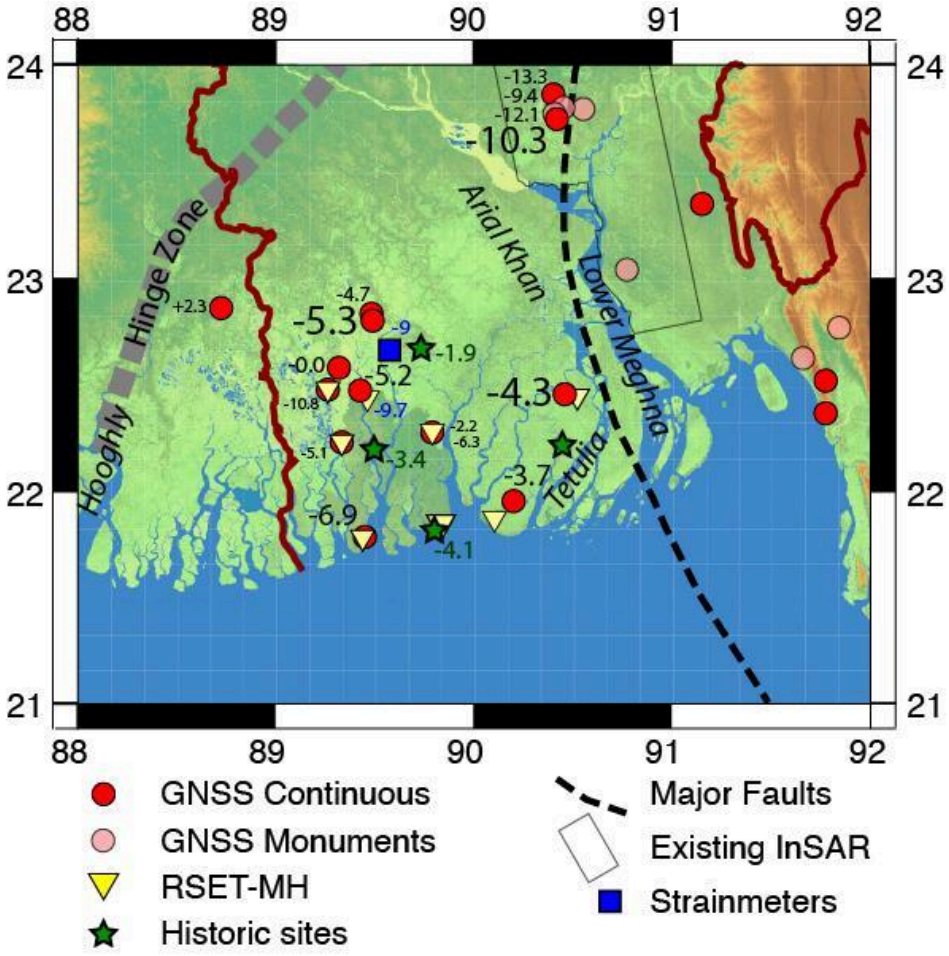

Figure 1. *Subsidence rates in coastal GBD west of the deformation front (dashed line). Text size is proportional to the √(time series length) to represent the reliability of the values, except for historic sites. Historic sites values are similar to Holocene average rates (Grall et al., 2018). GNSS rates are similar to slightly higher, especially farther west. River names in italics. Values updated from Steckler et al. (2022).*

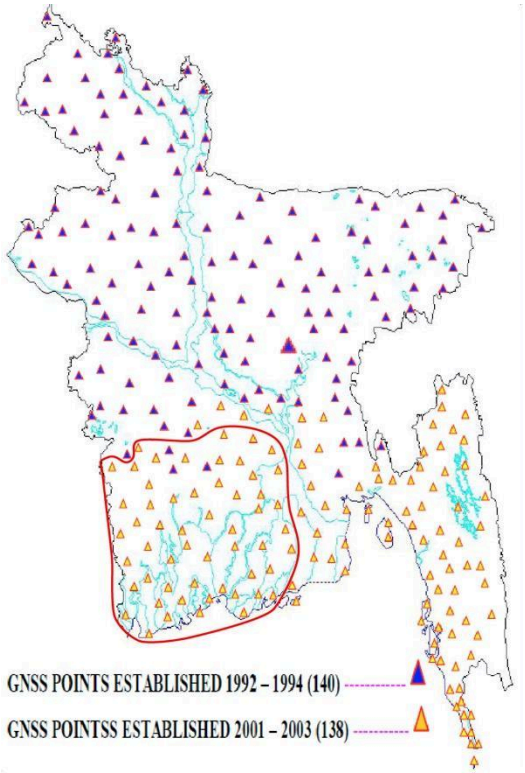

Figure 2. *Map shows the position of the 278 geodetic monuments installed by the SoB in conjunction with JICA. The 55 monuments targeted for reoccupation are enclosed in by red curve. 47 of the sites were successfully remeasured.*

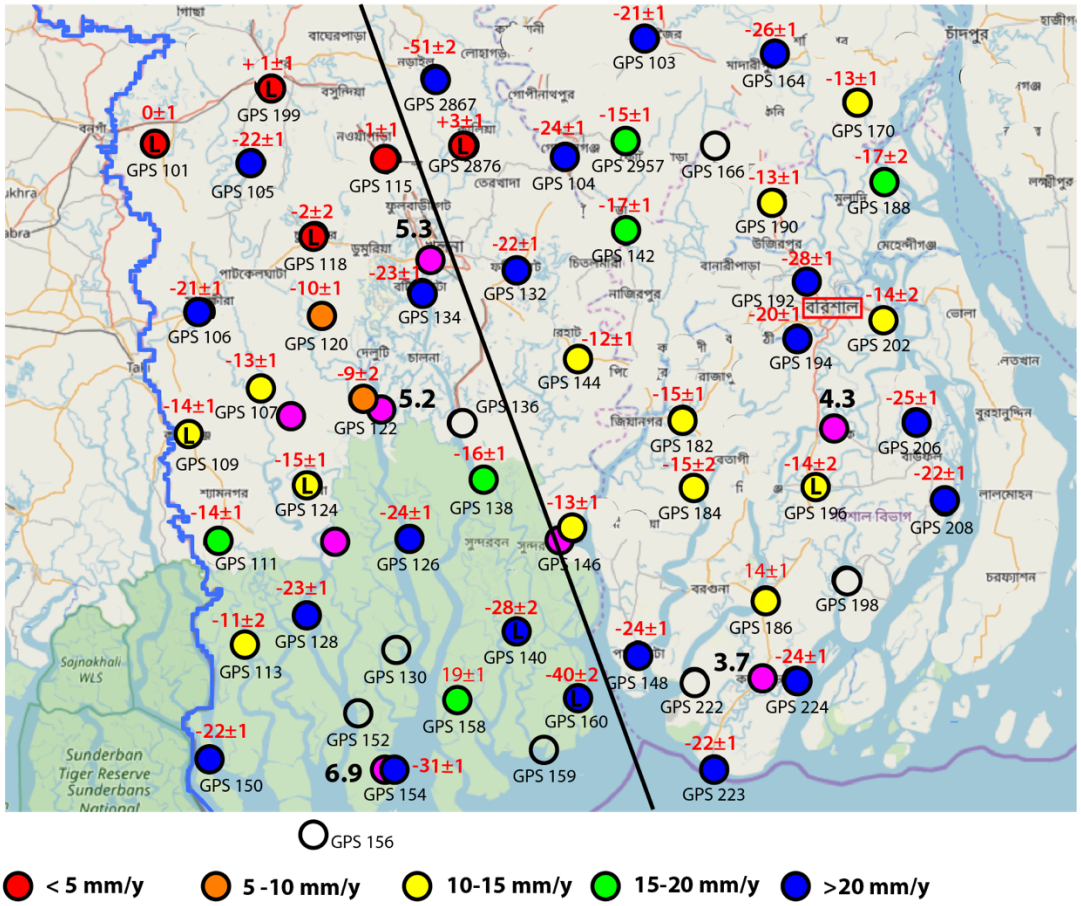

Figure 3. *The map shows the results for the 55 monuments targeted for reoccupation. 47 sites were successfully remeasured. The apparent subsidence rates are above and the site name are below the colored circles. The magenta circles are the positions of our continuous GNSS installations with the rate in bold. The green area on the background map is the Sundarban Mangrove Forest.*

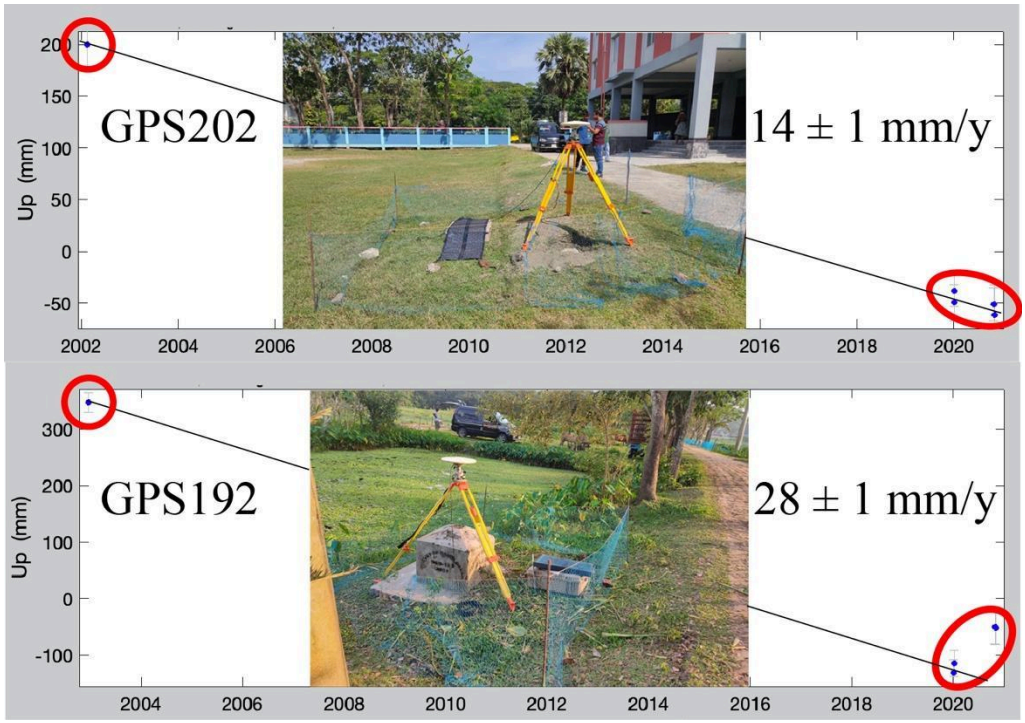

Figure 4. *Plots of the time series for two of the reoccupied campaign sites. For the site on the top, the three measurements are colinear. For the site on the bottom, the third measurements yielded uplift relative to the long-term trend. We suspect that this site has slumped and is now shifting vertically seasonally with the rice field. This supports our inference of monument instability.*

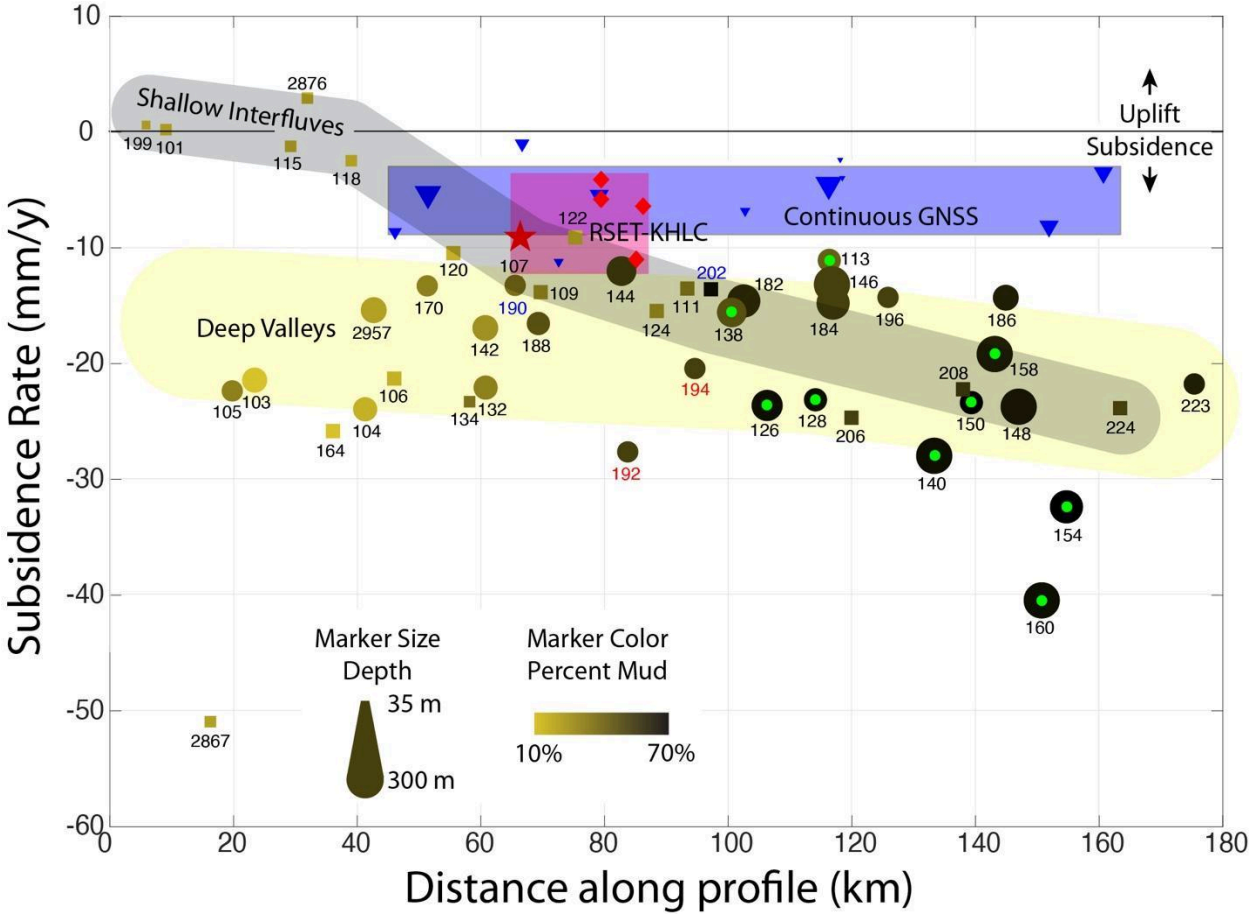

Figure 5. *Plot shows subsidence rates from the SoB monuments projected along a profile N160°E, perpendicular to the subsidence contours in Grall et al. (2018) and shown in Figure 3. Markers for sites with the estimated Holocene sediment thickness is less than 100 m are squares and where the thickness is greater thatn 100 m are circles. Sizes are proportional to estimates thicknesses, with considerable uncertainty for the larger thicknesses. The green dots correspond to sites within the Sundarban Mangrove Forest. The blue and red site labels correspond to the four sites where the resurvey yielded linear and nonlinear subsidence, respectively. Grey and yellow bands show the trends for the two sets. The shallow interfluves show increasing subsidence along the profile as the Holocene sediments become thicker and muddier. The deep valley sites yield only a slight increase along the profile. The symbol size for the blue continuous GNSS sites are proportional to the time series length (Steckler et al., 2022). The red diamond are the RSET rates corresponding to proximal and interior polder sites at 79 km and stream bank and interior Sundarban sites at 85 km (Akter et al., in press). The KHLC compaction meter results is given as a red star (Steckler et al., 2022). See text for discussion.*

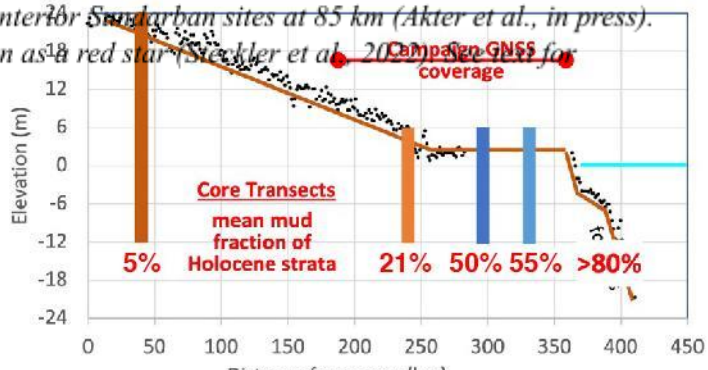

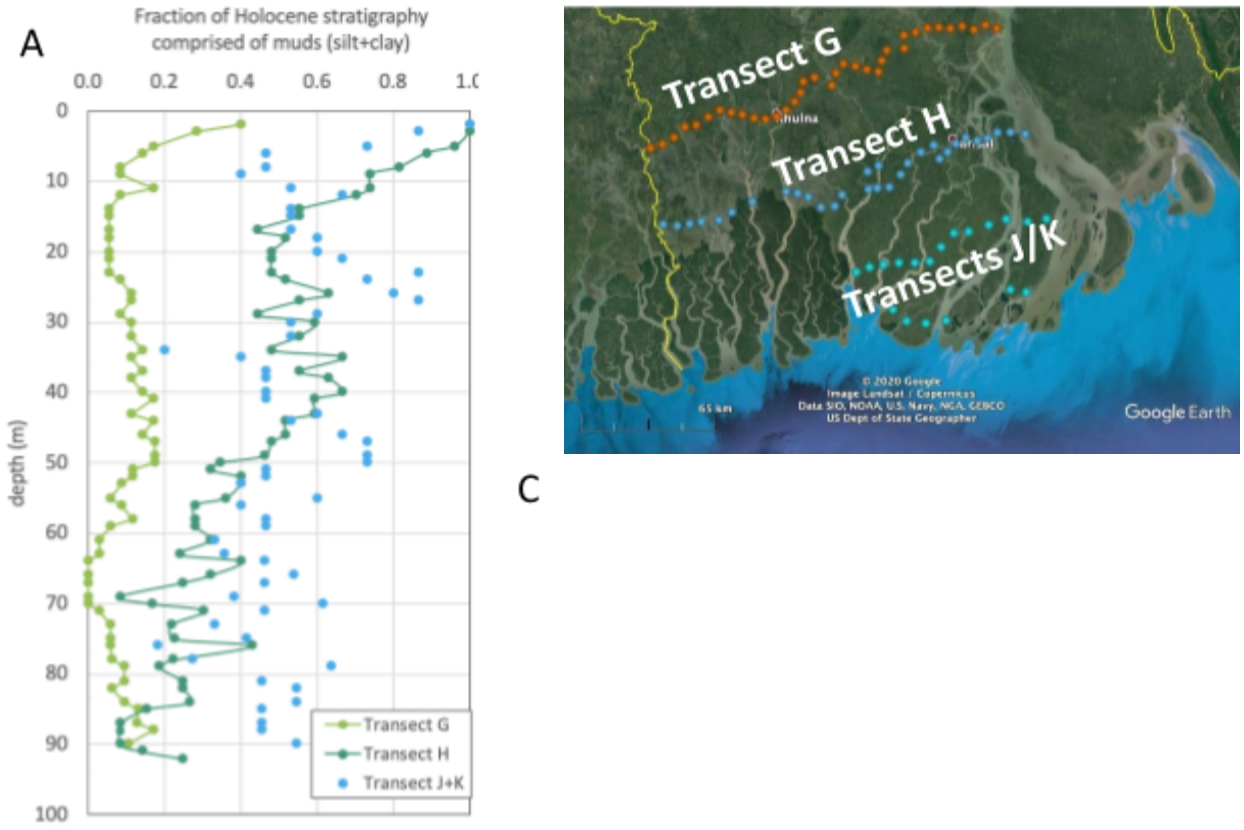

***Figure 6**. **A)** Average lithology versus depth across the lower delta for each of the transects located in B. **B)** Map showing the locations of the wells for each tube well transect. C) Cross section showing the increasing percentage of mud toward the coast. The topographic break corresponds to the fluvial to fluvio-tidal transition (Wilson and Goodbred, 2015) and a major increase in mud in the tidal zone of the delta.*

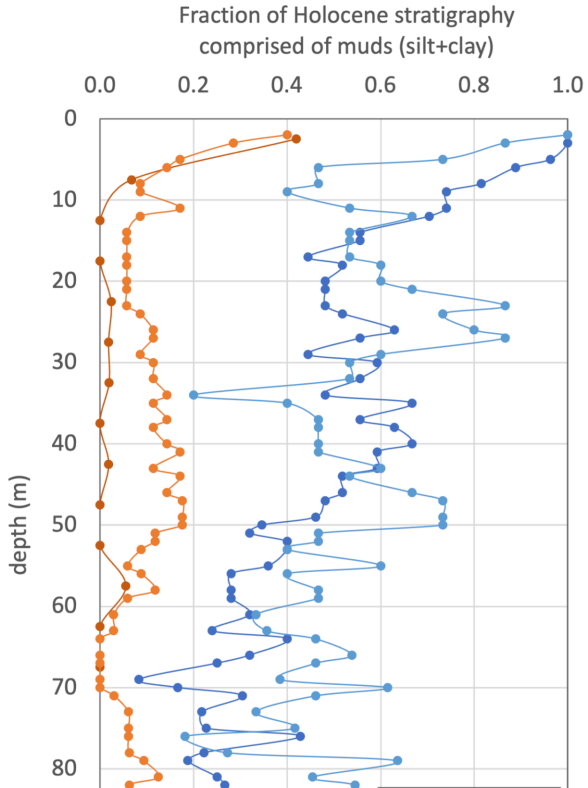

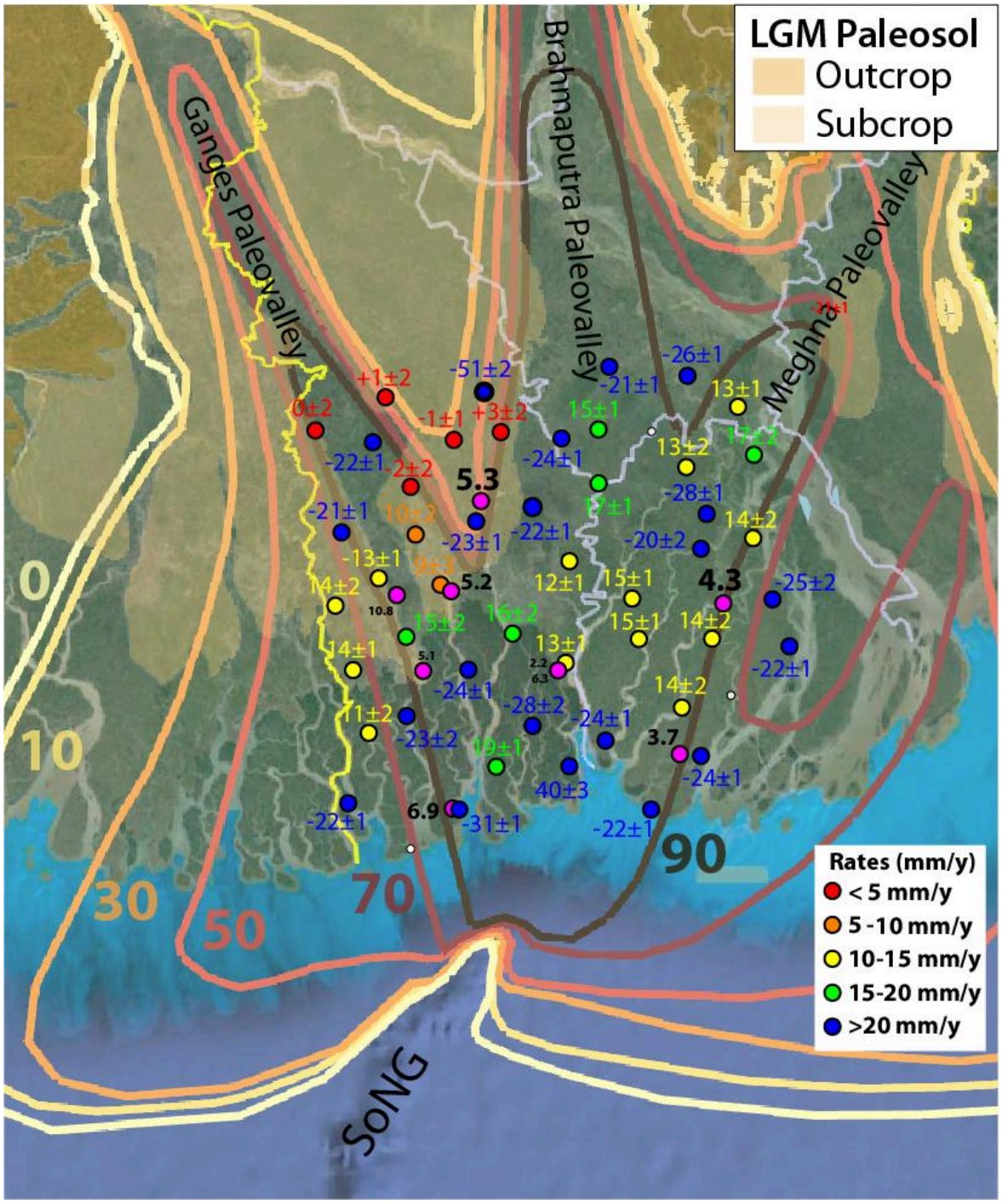
LGM Paleosol
Outcrop
Subcrop
Ganges Paleovalley
Brahmaputra Paleovalley
Meghna Paleovalley
SoNG
0
10
30
50
70
90
Rates (mm/y)
< 5 mm/y
5 -10 mm/y
10-15 mm/y
15-20 mm/y
>20 mm/y

Figure 7. Map showing the contours of the Holocene sediment thickness (Sincavage, 2017; Sincavage et al., 2017). The map shows that the major rivers incised significant valleys feeding into the shelf-indenting Swatch of No Ground (SoNG) canyon. Exposure and weathering of the interfluves created an oxidized clay paleosol that has been mapped by Hoque et al. (2014). Their mapped surface has been added in shades of brown. All of the low subsidence sites overly the thin Holocene overlying the LGMP while the higher rates are associated with thick sediments in the paleovalleys.

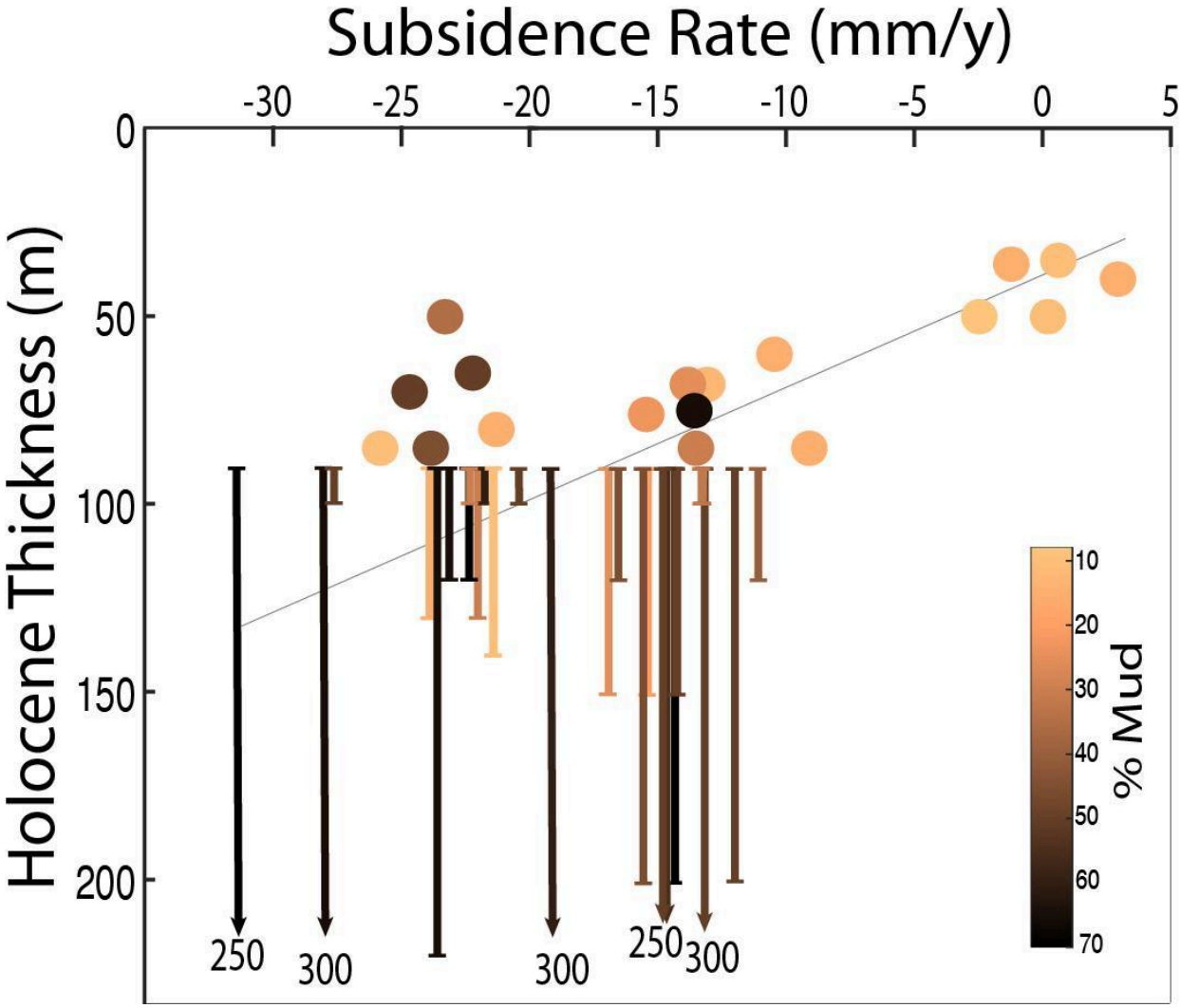

Figure 8. Plot of subsidence rate versus Holocene sediment thickness interpolated to the campaign GNSS sites. For sites where the sediment thickness is greater than the depth of tube wells, maximum depth was roughly estimated using the incised valley pathways to the SoNG canyon lowstand surface (Palamenghi, 2011). The range is indicated by arrows and labels. The symbols are colored by the percentage muds at the site interpolated from nearby tube wells.

Figure 9. Cartoon presenting a synthesis of subsidence versus depth based on combining measurements from multiple instruments, each of which measure compaction or subsidence over a different depth range. GNSS on building and tide gauges measure subsidence below the building or gauge foundations and miss shallow compaction. The RSET-MH and KHLC compaction meter measure compaction above the base of their instruments. The campaign GNSS on SoB monuments measures both shallow and deep subsidence. Combining the results, the synthesis column shows a preliminary estimate of subsidence in each depth range. The long-term rates correspond to the sum of the two deeper brown layers.

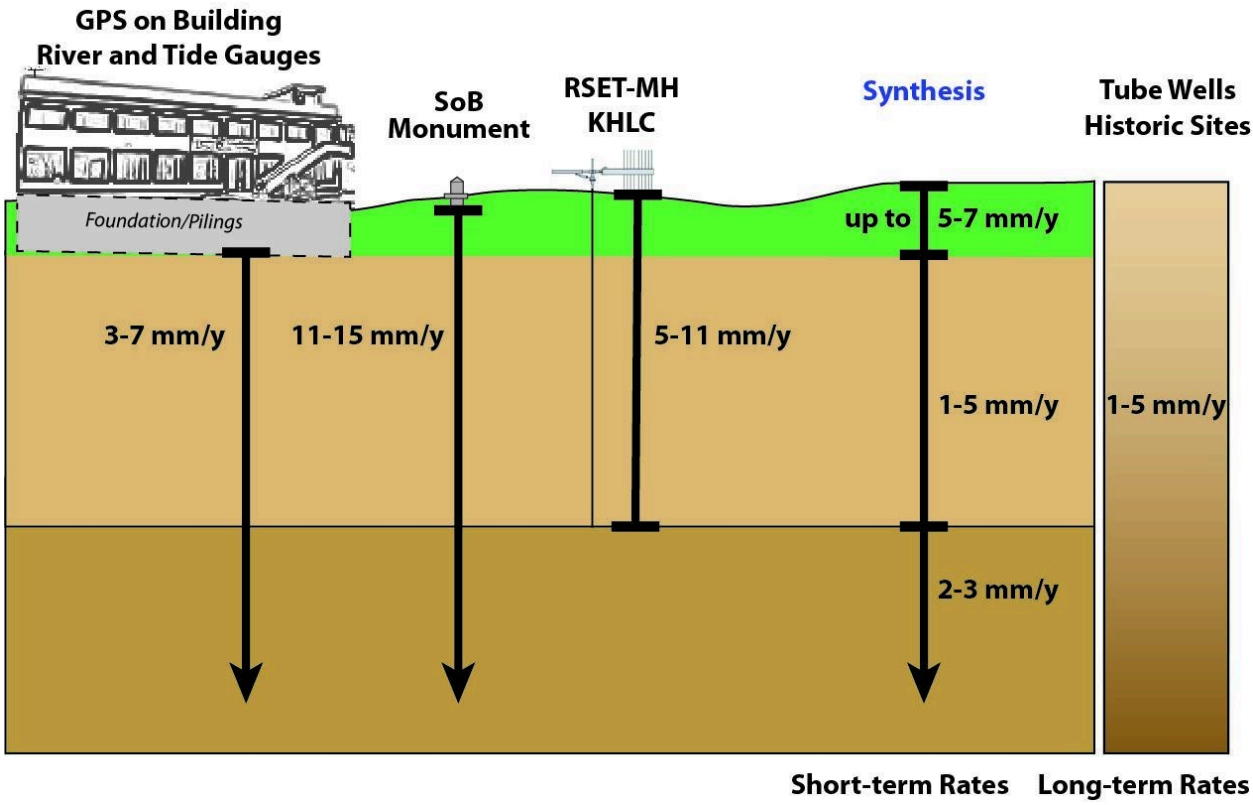
GPS on Building
River and Tide Gauges
SoB
Monument
RSET-MH
KHLC
Synthesis
Tube Wells
Historic Sites
Foundation/Pilings
up to 5-7 mm/y
3-7 mm/y
11-15 mm/y
5-11 mm/y
1-5 mm/y
1-5 mm/y
2-3 mm/y
Short-term Rates
Long-term Rates